International Journal of the Korean Society of Precision Engineering, Vol. 4, No. 3, May 2003.

Development of Hardware-in-the-Loop Simulation System for Use in Design and Validation of VDC Logics

Kihong Park[1] and Seung-Jin Heo[1,#]

[1] School of Mechanical and Automotive Engineering, Kookmin University, Seoul, South Korea

ABSTRACT

The objective of the Vehicle Dynamics Control (VDC) system is to maintain vehicle stability under critical lateral motions. It has a good potential of becoming one of the chassis control necessities since the system can be realized with little additional cost on top of the ABS/TCS system. Developed in this research is a hardware-in-the-loop simulator for VDC with a valve control system that modulates the brake pressures at four wheels. Two VDC control logics, a simple control logic and an LQR control logic, have been developed and incorporated in the HILS system. Their performance under various driving conditions was tested in the HILS system and the results are presented.

Key Words : Vehicle Dynamics Control, Hardware-in-the-Loop Simulation

1. Introduction

Efforts are being made actively in automotive industries to develop the VDC system whose objective is to maintain the lateral vehicle stability in critical cornering situations[1-3]. Some of the systems have been successfully commercialized for passenger vehicles. The VDC system has a good potential of becoming one of the chassis control necessities since the system can be realized with little additional cost on top of the ABS/TCS system.

A critical lateral motion of a vehicle occurs when tire-road contactness cannot be sustained. When this occurs, the body sideslip angle grows and the sensitivity of the yaw moment with respect to the steer angle suddenly diminishes. Addition of the steer angle can no longer increase the yaw moment which is necessary to restore the vehicle stability. In such situations, the VDC system tries to make the vehicle's lateral motion behave as closely as the driver's steering intention. To this end, the VDC generates a compensating yaw moment to restore the stability by distributing asymmetric brake forces to the wheels.

Corresponding Author :
Email : sjheo@kookmin.ac.kr
Tel.+82-2-910-4713

In this research, two VDC control logics have been designed, a simple controller and an LQR controller. Both controllers first compute the target yaw rate from the vehicle speed and steering angle, and then compute the compensating yaw moment. The simple controller computes the compensating yaw moment using the error between the actual yaw rate and the reference yaw rate, and then performs combined sequence of three pressure modulation modes - build, hold, and reduce - independently at four wheels. Asymmetric pressure distribution at four wheels generates the compensating yaw moment. The LQR controller computes the compensating yaw moment by a state feedback control law.

The hardware-in-the-loop simulation (HILS) scheme is being widely adopted in automotive industries[4,5]. It integrates the actual ECU and its peripheral hardwares with the virtual vehicle model, forming a closed loop to be simulated in real time. The result of the HIL simulation has better credibility than that from pure numerical simulation. HILS provides better time- and cost-effectiveness over actual driving test. It also makes possible test procedures that are difficult or even impossible in actual driving tests. Such advantages are especially favorable for brake control ECU's since their in-vehicle tests are characterized by high cost, long test period, and potential danger of the test.

With the motivation explained above, a HILS system has been developed that can be used for validating the VDC control logics when the control logics are implemented on a PC. The system consists of three parts; the hardware part which includes the hydraulic system that ranges from the brake pedal and master cylinder to the four wheel cylinders, the software part which includes the vehicle model, the VDC control logics, and post-processing module, and interface part which links the hardware and software parts.

Pressure modulation device is needed to incorporate a PC controller in the VDC HILS environment. A valve control system has been developed in this study to independently control the brake pressures at four wheels. The system has been built upon the HCU part of a commercial ABS module. It modulates the pressure of each wheel with two solenoid valves, inlet and outlet valves. Each solenoid valve is driven by a PWM signal.

The performance of the two controllers has been tested in the VDC HILS system under various driving conditions, and the results are presented and discussed in this paper.

2. Mathematical Models

2.1 Plant Vehicle Model

A seven degree-of-freedom vehicle model was used for the plant model in this study. It gives good description of the vehicle's lateral motion with simplicity. The model consists of a sprung mass that translates in longitudinal and lateral axes and that rotates about the vertical axis, and four unsprung masses that rotate about their own spindle axes. Fig. 1 shows the vehicle model and Eq. 1 gives its equations of motion[6].

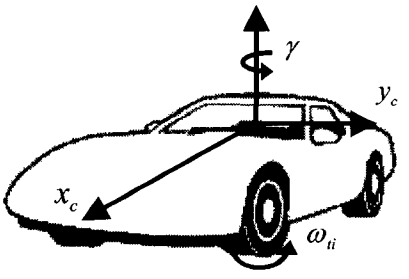

Fig. 1 Plant vehicle model

$$M_c(\ddot{x}_c - \gamma \dot{y}_c) = \Sigma F_{xti} \quad (1a)$$

$$M_c(\ddot{y}_c + \gamma \dot{x}_c) = \Sigma F_{yti} \quad (1b)$$

$$I_c\dot{\gamma} = l_f \sum_{1,2} F_{yti} - l_r \sum_{3,4} F_{yti} - \frac{l_t}{2}\sum_{1,3} F_{xti} + \frac{l_t}{2}\sum_{2,4} F_{xti} \quad (1c)$$

$$I_{ti}\dot{\omega}_{ti} = T_{bi} + T_{VDCi} + r_{ti}F_{xti} \quad (1d)$$

In the above, M_c represents the sprung mass, I_c the yaw moment inertia of the sprung mass, $\dot{x}_c$ the longitudinal velocity, $\dot{y}_c$ the lateral velocity, and γ the yaw rate. The subscript i is used for denoting a particular one out of 4 wheels: starting from i= 1, wheels are referred in the order of FL, FR, RL, and RR. F_{xti} and F_{yti} are, respectively, the longitudinal and lateral forces of each tire. The quantity I_{ti} is the rotational moment of inertia of the tire, ω_{ti} the rotational speed of the tire, r_{ti} the tire radius, l_f and l_r the distance from CG to the front and rear axles, respectively, and l_t the tread. T_{bi} is the brake torque from the driver and T_{VDCi} is the brake torque from the controller for generating the compensating yaw moment.

The vehicle model in this section was used only as the plant model. For controller design, a simpler vehicle model was used for facilitating the controller design process, which will be introduced in 3.1.

2.2 Tire Model

In this study, the brush tire model has been used for the plant vehicle model. Eq. 2 shows the mathematical equations of the brush tire model[7].

if $\varepsilon_i \geq 0$

$$F_{xti} = -K_{\lambda i}\lambda_i\varepsilon_i^2 + 6\mu_i F_{zti}\cos\theta_i(\varepsilon_i) \quad (2a)$$

$$F_{yti} = K_{\alpha i}(1+\lambda_i)\tan\alpha_i\varepsilon_i^2 - 6\mu_i F_{zti}\sin\theta_i f(\varepsilon_i) \quad (2b)$$

else if $\varepsilon_i < 0$

$$F_{xti} = \mu_i F_{zti}\cos\theta_i \quad (2c)$$

$$F_{yti} = -\mu_i F_{zti}\sin\theta_i \quad (2d)$$

where

$$\gamma_i = \sqrt{\lambda_i^2 + \left(\frac{K_{\alpha i}}{K_{\lambda i}}(1+\lambda_i)\tan\alpha_i\right)^2}\ ,\ \varepsilon_i = 1 + \frac{K_{\lambda i}\gamma_i}{3\mu_i F_{zti}}$$

$$f(\varepsilon_i) = \frac{1}{6} - \frac{1}{2}\varepsilon_i^2 + \frac{1}{3}\varepsilon$$

$$\sin\theta_i = \frac{K_{\alpha i}\tan\alpha_i(1+\lambda_i)}{K_{\lambda i}\gamma_i}\ ,\ \cos\theta_i = \frac{\lambda_i}{\gamma_i}$$

In the above, K_α and K_λ are tire characteristic

coefficients, λ the wheel slip ratio, μ the road friction coefficient, and α the wheel sideslip angle.

For the reference vehicle model, the simple saturation tire model[8] was used instead of the brush tire model since the former is easy to handle in the linear optimal controller design. Eq. 3 shows the equations of the simple saturation tire model.

$$F_{yti} = K_{\alpha i}\frac{\mu_i}{C_i}\tan^{-1}\left(\frac{C_i}{\mu_i}\alpha_i\right),\ C_i = \tau\frac{K_{\alpha i}}{F_{zti}} \tag{3}$$

The simple saturation tire model in this study was tuned to the brush tire model at the slip ratio of 0.01. From Fig. 2, it can be seen that the lateral tire forces of the two tire models agree well in both low and high friction roads. As the slip ratio grows, the discrepancy was observed to grow but it was kept within tolerable range.

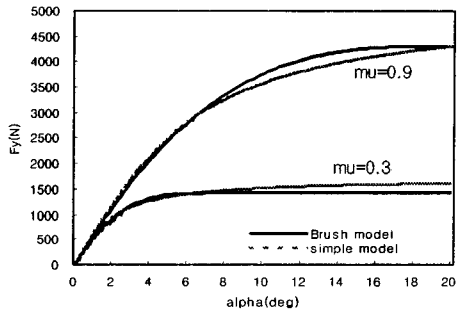

Fig. 2 Comparison of brush tire model and simple saturation tire model at λ =0.01

3. Controller Design

In this study, two controllers - a simple controller and an LQR controller - have been developed for VDC to compute the compensating yaw moment, and they are explained in this chapter.

3.1 Reference Vehicle Model

This section describes the reference vehicle model that was used in the VDC controllers as a substitute for the plant vehicle model in Fig. 1. The simple controller uses the reference vehicle model when computing the reference yaw rate, that is, the target yaw rate to follow. The LQR controller uses the reference vehicle model to construct a state feedback control law since the controller designing process becomes simpler and more straightforward when using this model instead of the plant vehicle model in Eq. 1.

Fig. 3 shows the reference vehicle model. This is a 2 degree-of-freedom bicycle model with its dynamics described by the lateral velocity and the yaw rate. Eq. 4 gives the equations of motion[9].

$$M_c(\dot{v}_y + v_x\gamma) = F_{ytf} + F_{ytr} \tag{4a}$$

$$I_c\dot{\gamma} = l_f F_{ytf} - l_r F_{ytr} + T_z \tag{4b}$$

In the above, T_z is the compensating yaw moment generated by the asymmetric braking force distribution from the VDC system.

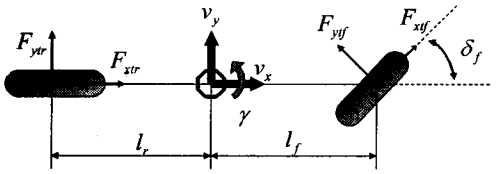

Fig. 3 Reference vehicle model

3.2 Simple Controller

The simple controller first computes, using the vehicle model in Fig. 3, the reference yaw rate. This is the steady state yaw rate at current values of the vehicle speed and the steer angle input, and is given in Eq. 5.

$$\gamma_{ref} = \frac{v_x}{(l_f + l_r)\left(1 + \frac{v_x^2}{v_c^2}\right)}\delta_f \tag{5}$$

In the above, γ_{ref} is the reference yaw rate and v_c the charateristic speed of the vehicle.

Table 1 Control scheme of simple controller

$\gamma_{act} - \gamma_{ref} > 0$	$\delta \geq 0$		
	$\delta < 0$		
$\gamma_{act} - \gamma_{ref} < 0$	$\delta \geq 0$		
	$\delta < 0$		
$\gamma_{act} - \gamma_{ref} = 0$	any δ		HOLD MODE

Plant vehicle (7dof) Reference vehicle (2dof)

The controller then compares the actual yaw rate of the plant vehicle model with the reference yaw rate that was computed from the reference vehicle model. Based upon the error between the two values, it computes the compensating yaw moment, and to achieve this, it performs combined sequence of three pressure modulation modes - build, hold, and reduce - independently at four wheels. This is similar to one of the well-known Bosch ABS logics[10]. The duty ratios for the PWM signals that drive the on-off solenoid valves are set at constant values in each mode.

Table 1 shows the control scheme of the simple controller. The compensating yaw moment is generated by applying brake force only at either left or right side of the vehicle. And the brake force at the controlled side is distributed to the front and rear wheels in a certain ratio.

3.3 LQR Controller

This section describes the vehicle dynamics controller that has been developed using the linear quadratic regulator (LQR) theory. The controller is built upon the simplified vehicle model in Eq. 4 and the simple saturation tire model in Eq. 3. Eq. 6 shows the linearized state equation of the reference vehicle model.

$$\dot{x} = Ax + BT_z + E\delta_f \tag{6}$$

where $x = \begin{bmatrix} v_y \\ \gamma \end{bmatrix}$,

$$A = \begin{bmatrix} \frac{1}{M_c}\frac{\partial(F_{ytf}+F_{ytr})}{\partial v_y} & \frac{1}{M_c}\frac{\partial(F_{ytf}+F_{ytr})}{\partial \gamma} - v_x \\ \frac{1}{I_c}\frac{\partial(l_f F_{ytf} - l_r F_{ytr})}{\partial v_y} & \frac{1}{I_c}\frac{\partial(l_f F_{ytf} - l_r F_{ytr})}{\partial \gamma} \end{bmatrix}$$

$$B = \begin{bmatrix} 0 & \frac{1}{I_c} \end{bmatrix}^T, \quad E = \begin{bmatrix} \frac{1}{M_c}\frac{\partial F_{ytf}}{\partial \delta_f} & \frac{l_f}{I_c}\frac{\partial F_{ytf}}{\partial \delta_f} \end{bmatrix}^T$$

In the above, the compensating yaw moment T_z is the control variable and the steer angle δ_f is treated as a disturbance. Eq. 7 shows the state feedback control law that can compensate for the steady state offset induced by a nonzero δ_f.

$$T_z = T_{x_d} - C_x(x - x_d) \tag{7}$$

In the above, x_d is the desired steady state for a given δ_f and T_{x_d} is the compensating yaw moment necessary to yield x_d. These desired quantities are computed from Eq. 6 with the assumption of steady state cornering, and they are given in Eq. 8.

$$x_d = -C_x\delta_f, \; T_{z_\delta} = -C_{T_\delta}\delta_f \tag{8}$$

By substituting Eq. 8 in Eq. 7, the following control law is obtained.

$$T_z = -C_x x - C_\delta \delta_f \tag{9}$$

where $C_\delta = C_{T_\delta} - C_x C_{x_\delta}$

Eq. 9 represents a controller that consists of a state feedback controller and a feedforward controller. The feedback gain matrix C_x in Eq. 9 has been computed using the LQR theory. The feedforward gain C_δ is computed by Eq. 9 once C_x is determined. Fig. 4 shows the block diagram of the overall closed loop system.

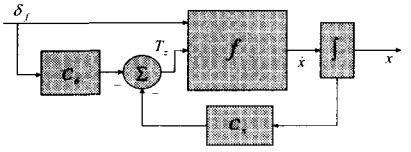

Fig. 4 Block diagram of LQR-based VDC

Eq. 10 shows the performance index that was used to exploit the LQR theory.

$$PI = \int_0^\infty (x^T Q x + r T_z^{\,2})dt \tag{10}$$

In the above, Q is a penalty weight matrix for the state variables and r is a penalty weight for the control usage. When Q is positive semi-definite and r is positive, and when the system in Eq. 6 is controllable, a steady state controller gain C_x can be obtained which minimizes the given performance index. The system in Eq. 6 satisfies the controllability condition. Eq. (11) shows Q and r used in this study.

$$Q = \begin{bmatrix} 5\times10^{10} & 0 \\ 0 & 0.1\times10^{10} \end{bmatrix}, \quad r = 1 \tag{11}$$

3.4 ABS Controller

As previously seen, the compensating yaw moment is generated by asymmetric brake pressures at four wheels. But when the brake pressure is excessive at a certain wheel, the wheel gets locked and the braking force diminishes, which, in turn, degrades the

performance of the VDC system. Hence it is important to maintain the wheel slip ratio at its optimum so that the maximum brake force is achieved despite excessive brake pressure. To this end, the Bosch ABS logic was implemented by an algorithm and integrated with the two VDC controllers[10].

4. HILS System

This chapter describes the HILS system that has been developed in this research for testing the PC-based VDC control logics. The system consists of three parts; hardware part, software part, and interface part. The HIL simulation was implemented at the sampling rate of 5ms. Fig. 5 shows the configuration of the system. Details for each part are explained below.

Hardware Part. This part is basically composed of hydraulic devices for the brake system. First it includes the brake pedal, the master cylinder, the vacuum booster, hydraulic tubes; and the wheel cylinders and brake discs for each wheel. To provide vacuum to the vacuum booster without an engine, a vacuum pump is installed.

A valve control system has been developed in this study. This is needed since, in the HILS system of this paper, the VDC logic was implemented as software while the hydraulic system resides as hardware. The valve control system consists of 8 solenoid valves. The brake pressure of each wheel is modulated by one inlet and one outlet solenoid valves. The solenoid valves are on-off type, and there are three pressure modulation modes; build, hold, and reduce. The build mode is achieved with inlet open and outlet closed, the hold mode with inlet closed and outlet closed, and the reduce mode with inlet closed and outlet open. The valves are controlled by PWM signals. In the simple controller, the duty ratio of the PWM signal is predetermined for each pressure modulation mode. In the LQR controller, the duty ratio changes according to the control demand. Currently the valve control system does not have its own pressure build-up mechanism. So the VDC logics of this study were tested only when the operator applied the brake pedal.

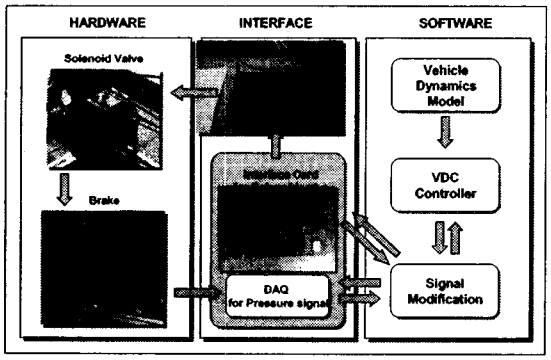

Fig. 5 Configuration for VDC HILS system

Software Part. This part consists of the vehicle model the VDC controllers, real-time simulation part, and the post-processing part. A sampling time of 5ms was achieved on a Pentium 3 platform. The post-processing part provides visualization of vehicle response.

Interface Part. This part links the hardware part with the software part. First, interface is needed to provide linkage between the actual brake system and the virtual vehicle dynamic model. For this, a pressure sensor was installed at the entrance of each wheel cylinder. The pressure measurements are fed to the computer via A/D channels, and then converted into brake torques, and then fed to the vehicle dynamic model as system inputs. The pressure of the master cylinder was also measured for the purpose of validation. This forms a passage from hardware to software in the closed loop of the VDC HILS. The passage from software toward hardware is formed by sending out the controller output in the PC to the valve control system outside the PC. Since the valve control system has the PWM signal generating circuit, the PC sequentially sends out 8 bit digital signals for each valve via PCI port.

Fig. 6 shows the VDC HILS system built in this research.

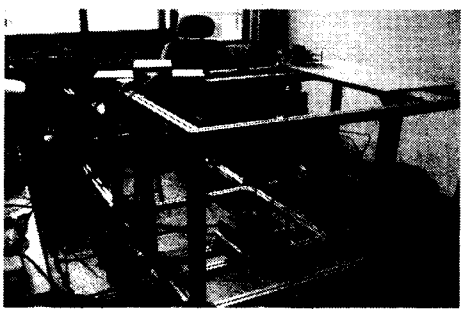

Fig. 6 VDC HILS system

5. Simulation

This chapter shows results of the hardware-in-the-

loop (HIL) simulation that has been conducted for performance validation of both the controllers and the VDC HILS system. Since the VDC system in practice operates near critical driving situations, simulation was performed for potentially dangerous situations. The tests include J-turn and slalom with high vehicle speed on a slippery road.

5.1 J-turn test

A J-turn test was performed under the following conditions. The road friction coefficient is 0.3, the initial vehicle speed is 100 km/h, and the steer angle goes through a step change of 5 deg. Fig. 7 and Fig. 8 show the pure simulation result and the HIL simulation result, respectively, for the two VDC controllers. The simulation result without any controller is also shown for comparison.

The graphs from the pure simulation in Fig. 7 display similar trend to those from the HIL simulation in Fig. 8, but the driving distances from the HIL simulation are shorter than those from the pure simulation. In the pure simulation, the brake torques at the uncontrolled wheels, which are the outside wheels, become zero as soon as the VDC starts to operate. In the HIL simulation, however, it takes some time to reduce the brake pressures at those wheels. Also in the HIL simulation, braking performance is better with the help of ABS than in the pure simulation that runs without ABS.

It is observed that both controllers yield better cornering performance with less drift than the case without any VDC controller, and among the two controllers, the LQR controller is better than the simple controller. At the end of the HIL simulation in Fig. 8, the two controllers yield vehicle locations as remote as 60m apart, and this implies significant safety improvement with the LQR controller.

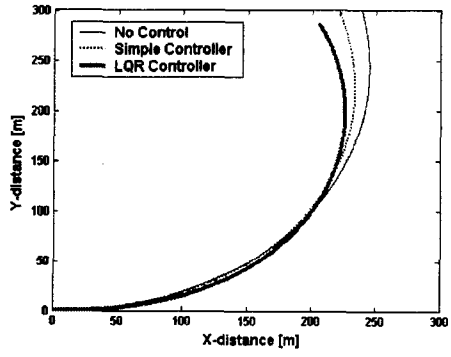

Fig. 7 Vehicle trajectory in J-turn in pure simulation

Fig. 7 Vehicle trajectory in J-turn in pure simulation

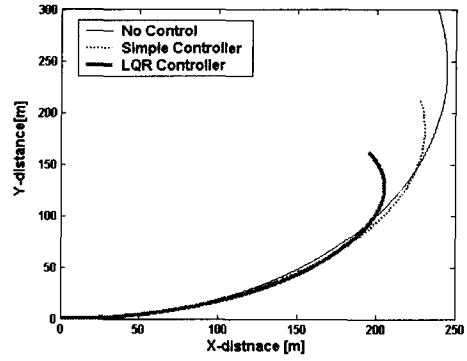

Fig. 8 Vehicle trajectory in J-turn in HIL simulation

5.2 Slalom test

A slalom test was performed under the same condition as the J-turn test. The steer angle goes through a sinusoidal change with the frequency of 0.25Hz and the amplitude of 5 deg. Fig. 9 and Fig. 10 show the pure simulation result and the HIL simulation result, respectively.

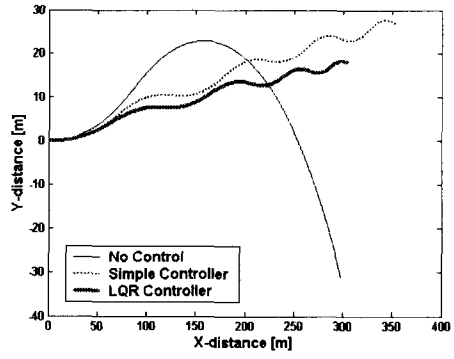

Fig. 9 Vehicle trajectory in slalom in pure simulation

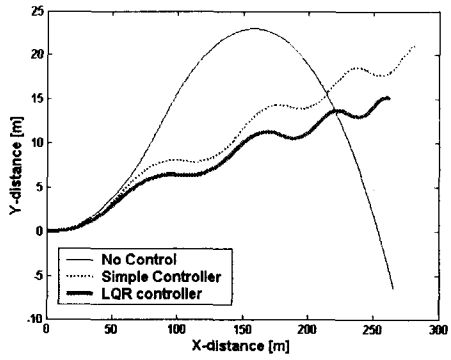

Fig. 10 Vehicle trajectory in slalom in HIL simulation

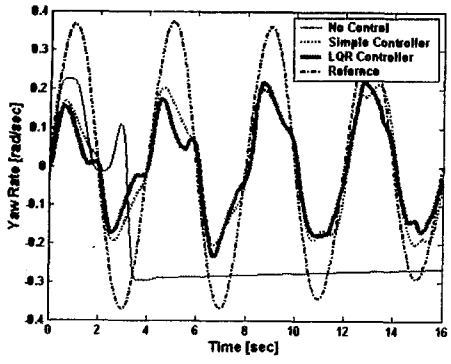

Fig. 11 Yaw rate in slalom in HIL simulation

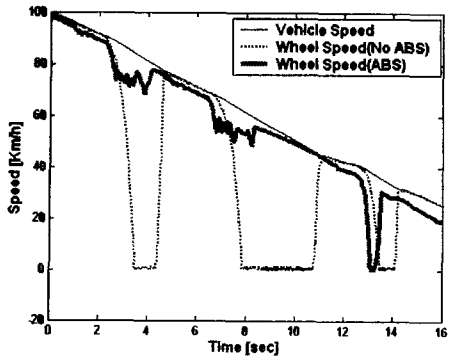

Fig. 13 Wheel speeds in slalom with and without ABS

It is seen that both controllers follow the driver's steering intention well while the vehicle without any VDC controller diverges. Among the two controllers, the LQR controller gives better tracking capability than the simple controller. The LQR controller yields shorter traveling distance than the simple controller since the former can yield desired braking torque more quickly. At the end of the HIL simulation in Fig. 10, the LQR controller gives lateral vehicle location 7m less than that by the simple controller.

Fig. 11 shows time histories of the yaw rate in the HIL simulation. When there is no control, the yaw rate fails to follow the desired(reference) yaw rate after 2 seconds from start. The yaw rates for the two controllers follow the reference yaw rate with little phase lag. The magnitudes of the yaw rates for the two controllers, however, fall short of the magnitude of the reference yaw rate, and this is because the reference yaw rate does not account for the slippery road condition.

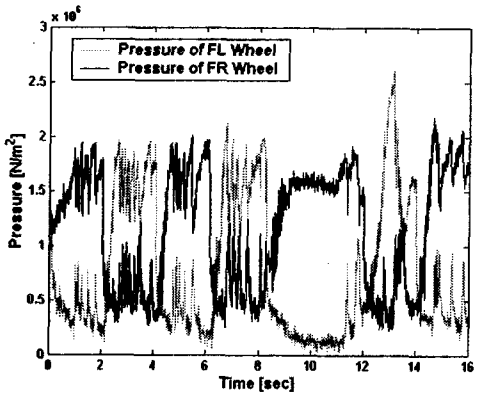

Fig. 12 Brake pressures in slalom in HIL simulation

Fig. 12 shows the brake pressures measured from the wheel cylinders at the front-left and front-right wheels in the slalom test for the LQR controller. When the pressure in one side increases, the pressure in the other decreases, and vice versa. By repeating this out-of-phase activity, the LQR controller maintains stability despite the harsh driving condition in the slalom test.

Fig. 13 shows the vehicle speed and the wheel speeds in the slalom test for the two cases, one with ABS and the other without ABS. In both cases, the LQR controller is operating. It can be seen that the ABS helps preventing wheels from locking during the operation of VDC, and this enhances the performance of the VDC. It is observed that the periodic pattern in Fig. 12 momentarily disappears from 8 sec. This is due to the activity of ABS as can be seen in Fig. 13, which overrules VDC when the wheel gets locked.

6. Conclusion

In this research, two VDC controllers, a simple controller and an LQR controller, have been developed for improving vehicle stability in critical lateral motion. The simple controller compares the yaw rate with its reference value, and conducts one of three prescribed pressure modulations - build, hold, and reduce - based upon the error. The LQR controller was built upon a simplified vehicle model, and it computes the compensating yaw moment with the driver's steering intention under consideration.

Also developed is the hardware-in-the-loop simulation system for testing the VDC controllers. The

system consists of the hardware part with an actual hydraulic brake system and valve control system; the software part which contains the vehicle model, the VDC control logic, real-time simulation module, and post-processing module; and the interface part that links the hardware and software parts.

The HIL simulation under critical driving conditions was conducted to validate the performance of both the controllers and the VDC HILS system. From the simulation results, it was shown that the two controllers could successfully maintain the vehicle stability at harsh lateral driving conditions, which could have otherwise led to fatal accidents without the controllers. Among the two controllers, the LQR controller always gave better stability control over the simple controller. In the HIL simulation of J-turn, the terminal vehicle global location was different by 60m, and in the slalom test, the terminal vehicle lateral location was different by 7 m. From the test results, it was shown that integration of the ABS in the VDC system could enhance the performance of the VDC.

Acknowledgement

This research was supported by 2002 Brain Korea 21 Project.

References

1. Zanten, A. T. V., Erhardt, R., Pfaff, G., Kost, F., Hartmann, U., Ehret, T., "Control Aspects of the Bosch-VDC," Proceedings of AVEC, pp. 573-607, 1996.
2. Tseng, H. E., Ashrafi, B., Madau, D., Brown, T. A., Recker, D., "The Development of Vehicle Stability Control at Ford," IEEE/ASME Transactions on Mechatronics, Vol. 4, No. 3, pp. 223-234, 1999.
3. Park, K. and Heo, S. J., "Design of a Control Logic for Improving Vehicle Dynamic Stability," Proceedings of AVEC, pp. 577-584, 2000.
4. Boot, R. and Richert, J., "Automated Test of ECUs in a Hardware-in-the-Loop Simulation Environment," Proc. of the IEEE ISCACSD, pp. 587-594, 1999.
5. Lee, H. J., Park, Y. K. and Suh, M. W., "Development of Hardware-in-the-loop Simulator for ABS/TCS," Journal of the Korean Society of Precision Engineering, Vol. 16, No. 5, pp. 83-90, 1999.
6. Wong, J. Y., Theory of Ground Vehicles, 3rd Ed., Wiley, 2001.
7. Pasterkamp, W. R. and Pacejka, H. B., "The Tyre As A Sensor To Estimate Friction," Proceedings of AVEC, pp. 839-853, 1996.
8. Nagai, M., Hirano, Y. and Yamanaka, S., "Integrated Control of Active Rear Wheel Steering and Direct Yaw Moment Control," Vehicle System Dynamics, Vol. 27, pp. 357-370, 1996.
9. Matsumoto, S., Yamaguchi, H., Inoue, H. and Yasuno, Y., "Braking Force Distribution Control for Improved Vehicle Dynamics," Proceedings of AVEC, pp. 441-446, 1992.
10. Alder, U., Automotive Handbook, 3rd Ed., Robert Bosch GmbH, 1993.